Atomic force microscopy to assess the mechanical properties of individual casein micelles

Julien Bauland, Antoine Bouchoux, Thomas Croguennec, Marie-Hélène Famelart, Fanny Guyomarc'H

Atomic force microscopy to assess the mechanical properties of individual casein micelles

Julien Bauland [a,b], Antoine Bouchoux [c], Thomas Croguennec [a,*], Marie-Hélène Famelart [a], Fanny Guyomarc'h [a]

[a] INRAE, Institut Agro, STLO, 35042, Rennes, France
[b] Chr. Hansen 2970, Hoersholm, Denmark
[c] TBI, Université de Toulouse, CNRS, INRAE, INSA, Toulouse, France

ARTICLE INFO

ABSTRACT

Casein micelles (CMs) are ~100 nm natural colloids found in milk resulting from the complex and unresolved association of casein monomers, phosphorus, and calcium; the latter being either directly bound to the phosphoserine residues of caseins or present as nanoclusters of insoluble micellar calcium phosphate (MCP). Dairy products such as cheese or yogurt are colloidal gels formed by CMs destabilization, for which texture and ability to be processed are essentially determined by rheological properties. Those properties depend on the physico-chemical conditions used during gel formation (e.g., pH, temperature, ionic content). However, questions remain about the origin of this dependence at the microscopic scale. In particular, we still do not have a clear picture of the specific contributions of the rigidity of the elementary bricks (CMs) in comparison with the inter-particles interactions or their spatial distribution. In this work, Atomic Force Microscopy (AFM) is used to evaluate changes in the nanomechanical properties of single CMs following physico-chemical modifications that are known to affect the MCP content and the rheology of the enzymatic milk gel (i.e. decrease of pH and CaCl$_2$ addition). AFM is used as a direct indenter that assesses the CMs' elastic deformation and gives an estimate of their Young modulus. We show that for a ±18–24% w/w depletion or enrichment in MCP content, the Young modulus of CMs significantly decreases or increases, respectively. This correlation suggests that variations in the modulus of individual CMs could explain the changes in the macroscopic properties of the enzymatic milk gel upon variations of physico-chemical conditions.

1. Introduction

Caseins are phosphorylated, 19–25 kDa proteins that represent 80% w/w of the protein fraction in bovine milk. They naturally interact with minerals, principally calcium and phosphate in milk, to form colloidal structures of ~100 nm diameter that are referred to as casein "micelles". The internal structure of the casein micelle (CM) is still a subject to debate, but it is admitted that it contains micellar calcium phosphate (MCP) in the form of 4–5 nm "nanoclusters" that are stabilized by the phosphoserine residues of the caseins (Holt et al., 2013; David S. Horne, 2020). Depending on the model considered, there are ~800 to several thousand of nanoclusters per CM, each interacting with several phosphoserine residues. They can be viewed as cross-link elements of the CM internal structure as they form junctions between casein monomers. Some calcium ions, referred to as "calcium-bound" (Ca-bound), are also

directly bound to phosphoserine (and other acidic) residues of caseins, independently of the MCP clusters (Holt et al., 1986). The concentrations of MCP and of Ca-bound change upon variations of the milk physico-chemical conditions (Bauland et al., 2022). For example, decreasing of the milk pH reduces the ionization state of the phosphate ions and dissolves the MCP from the CMs into the aqueous phase, while the Ca-bound content increases following the increase in milk Ca^{2+} activity. On the opposite, CaCl$_2$ addition leads to the formation and precipitation of calcium phosphate into the CMs, increasing the MCP content. The Ca^{2+} activity and the Ca-bound also increase as only a fraction of the added calcium precipitates as MCP (Philippe et al., 2003). These changes are accompanied by changes in the concentration of soluble caseins and in the hydration degree of CMs.

The colloidal stability of CMs in milk at its native pH (6.7) arises from the κ-casein, located at the surface of the colloid. The C-terminal part of

---

κ-casein is highly charged and hydrated, providing steric and electrical repulsions (de Kruif, 1999). Milk gelation can be initiated by the addition of a proteolytic enzyme solution, called rennet, which specifically hydrolyzes the C-terminal part of κ-casein. Enzymatic gelation of milk is the first step of cheese making and understanding the mechanism of gel formation and aging has practical applications for the dairy industry. After enzymatic destabilization, the so-called para-κ-CMs aggregate and form a weak physical gel. The gel structure, initially diffuse, is transient and rearranges itself toward global compaction and coarser organization (Fagan et al., 2017). This phenomenon known as "micro-syneresis" is responsible for the increase in the shear modulus of the gel during aging. The partial fusion of the para-κ-CMs is assumed to be the driving force of the enzymatic gel aging (Mellema et al., 2002; van Vliet et al., 1991; Walstra et al., 1985) as hypothesized in model colloidal systems (Cipelletti et al., 2000).

Differences regarding the fusion of para-κ-CMs following variations of their MCP content are hypothesized to explain the effect milk physico-chemical changes on the enzymatic gel rheology (Cooke & McSweeney, 2014; Mellema et al., 2002). It is assumed that decreasing the MCP content of CMs by milk acidification or increasing it by CaCl$_2$ addition would respectively increase and decrease the fusion extent between particles, respectively and would be responsible of a change in the gel dynamic properties. Particle fusion is likely to depend on both inter-particle interactions and particle rigidity. While assumptions about inter-particle interactions can be made from the Ca^{2+} activity and the gelation temperature (Dalgleish, 1983; D. S. Horne & Lucey, 2014), the relation between CM rigidity and its MCP content has not been established yet. More generally, the link(s) between the macroscopic rheological properties of the gels and the microscopic properties of the CMs that constitute the gels are still missing (Mellema et al., 2002). Recently, it was shown that the extent of the macrosyneresis in colloidal gels was highly dependent on the deformability of the colloids, a property which is often overlooked (Wu et al., 2020). It highlights the necessity to determine if variations of the mineral content of CM, especially the MCP content, modify the particle rigidity.

One way to tackle this question is to directly measure the elastic properties of single CMs in physico-chemical conditions that are known to lead to gels with different rheological properties. Such measurements, at the nanoscale and in liquid conditions, are now accessible using modern physics tools like atomic force microscopy (AFM). In the present study, AFM is used as a miniaturized indenter for assaying the mechanical properties of the CMs (Benitez & Toca-herrera, 2014; Kim et al., 2021; Obeid & Guyomarc'h, 2020). Yet, two research groups have performed thorough mechanical investigation of CMs using AFM. In their pioneering paper, Uricanu et al. (2004) at the University of Twente (NL) calculate the Young modulus of individual CMs in different conditions of pH and temperature. A few years later, Bahri et al. (2017, 2018) at the University of Montpellier (FR) also used AFM to calculate the Young modulus of CMs prior to and after cross-linking by the enzyme transglutaminase (TG). These two groups immobilized control and modified CMs onto functionalized glass slides and performed imaging and force measurements in the same experiment in order to indent the CMs individually at their apex. Additionally, mechanical properties of CMs can be apprehended by AFM imaging through the measure of their contact angle with the fixation substrate, as this angle depends on the surface forces and the elastic nature of the object (Evangelopoulos et al., 2012). The lower the contact angle, the more the particle spread over the surface, indicating either higher surface forces or a lower elastic component. However, this approach is more easily performed in air, after a drying step, as it is challenging to assess correctly a contact angle in liquid conditions with such a soft object as the CM (Silva et al., 2015).

In this work, we focus on two physico-chemical effectors that have opposite effects regarding the MCP content of CMs and that are highly relevant for the dairy industry:

(i) A decrease in pH from 6.6 to 6.0, which results in a decrease of MCP by 18% (see Table 1 in section 3.3.1). CMs in this condition are referred to as "MCP-depleted".

(ii) The addition of calcium chloride (+10 mM) which results in an increase of MCP by 24% (see Table 1 in section 3.3.1). CMs in this condition are referred to as "MCP-enriched".

In an original approach, direct AFM indentation measurements are performed using *force-mapping experiments* onto a single layer of CMs in order to calculate Young moduli without the requirement of precise imaging. The contact angle of dried CMs is also calculated at a lower coverage density, i.e., in conditions where the dimensions of scattered individuals can be measured. The Young modulus and the contact angle of the modified CMs are compared to control CMs (pH 6.6, no CaCl$_2$ addition) and to a positive control where intra-micellar interactions are reinforced by TG covalent cross-linking; the corresponding CMs being referred as "TG-treated" CMs.

2. Materials and methods

2.1. Casein micelle suspensions

The CM isolate (75.9% w/w caseins) was purchased from Ingredia Functional Ingredients (Promilk 852B, Arras, France). It is obtained by microfiltration and diafiltration of milk followed by spray-drying. With this process, the whey protein, lactose and mineral contents of milk are reduced and the CMs are assumed to preserve their native state.

CM suspensions (30, 70, 110 or 140 g kg^{-1}) were prepared in milk ultrafiltration permeate (MUF) by dispersing the appropriate amount of CM isolate into MUF at 40 °C. The suspensions were stirred at that temperature for 3 h and then left overnight under stirring at room temperature (~20 °C) to ensure complete rehydration and were used within a week. Powder dispersion in MUF rather than water maintains the mineral content of CMs. The MUF was obtained at the STLO Dairy Plateform by ultrafiltration of a pasteurized skim milk at 50 °C (membrane cut-off 10 kDa). The MUF was stored at 5 °C with 0.2 g.L^{-1} sodium azide, to ensure preservation until use.

2.2. Reconstituted skim milk and milk ultrafiltrates

The skim milk was prepared from a homemade low heat skim milk powder, reconstituted at 100 g.L^{-1} in ultrapure water as previously reported (Bauland et al., 2020). Skim milk powder was stirred during 2h30 at room temperature with 0.2 g.L^{-1} sodium azide and then left overnight at room temperature. The milk pH was adjusted to 6.6 using 1 M HCl solution. To prepare the MUF of the MCP-enriched or MCP-depleted CMs, 10 mM CaCl$_2$ and HCl were added to the skim milk, respectively, and left for overnight equilibration. Control skim milk, skim milk supplemented with 10 mM CaCl$_2$ and skim milk adjusted at pH 6.0 were ultracentrifuged at 100,000 *g* × 1h at 20 °C. The supernatants were collected and ultrafiltered onto 10 kDa MWCO Vivaspin centrifuge tubes (Sartorius, Göttingen, Germany) at 2000 g × 1h at room temperature to get the MUFs.

Table 1
Mineral content and diameter of the control and modified casein micelles (CMs) in suspensions. N = 6 for hydrodynamic radii determination (1 suspension × 2 dilutions × 3 measurements).

		MCP-depleted	Control	MCP-enriched
Mineral content	Ca-bound (mM)	4.6	3.9	5.1
	MCP (mM)	17.5	21.4	26.5
	% of control	−18	-	+24
Hydrodynamic radii (nm)		74 ± 4	76 ± 4	75 ± 2

2.3. Covalent immobilization of casein micelles by carbodiimide chemistry

Gold-sputtered glass slides (Platypus Technologies LLC, Madison, WI, USA) were cut into ~1 cm square chips, washed with absolute ethanol and immersed into 2 mM mercaptoundecanoic acid in absolute ethanol for at least 24h at room temperature. The carboxyl-coated chips were thoroughly rinsed with absolute ethanol, then left to dry prior to being glued onto the middle well of a diagnostic microscope slide (Thermoscientific, Braunschweig, Germany). After curing and evaporation of the solvents, the chips (Fig. 1G) were stored in a desiccator until use. After rinsing with ultrapure water, the chips were covered with an extemporaneous mixture (1:1 v:v) of 0.1M N-hydroxysuccinimide and 0.4M 1-ethyl-3-(3-dimethylaminopropyl)-carbodiimide to activate the carboxyl groups for 30 min at room temperature

(A) Gold-MUA surface

(B) +30 g.kg⁻¹ CM

(C) +70 g.kg⁻¹ CM

(D) +110 g.kg⁻¹ CM

(E) +140 g.kg⁻¹ CM

(F) Topography and section

(G) gold-coated chip

Fig. 1. Surface coverage of the functionalized gold surface after reaction with 0–140 g kg⁻¹ casein micelles (CM) suspensions. (A)–(E) Amplitude 10×10 μm² images of functionalized gold-COOH surfaces with 0–140 g kg⁻¹ CM suspensions, showing the background surface on a 2×2 μm² scratched area at the center of the images. (F) Height image corresponding to the amplitude image (D) at 110 g kg⁻¹ CM, with the profile of a section drawn along the blue line. (G) Gold-coated chip glued on a glass slide. (For interpretation of the references to colour in this figure legend, the reader is referred to the Web version of this article.)

(Martin et al., 2006; Uricanu et al., 2004). The chips were thoroughly rinsed with ultrapure water and a CM suspension (30, 70, 110 or 140 g kg⁻¹) was deposited on the activated surface for 1h at room temperature. From the results of section 3.1, only CMs fixed at either 30 g kg⁻¹ or 110 g kg⁻¹ were then modified for imaging and indentation measurements, respectively.

2.4. In-situ modification of casein micelles

After exposition to CMs, the chips were gently rinsed with reconstituted skim milk to restore CMs in their natural mineral and protein equilibria. Control CMs were obtained by immersing the chips vertically in 30 mL of control skim milk during 1h with gentle stirring. MCP-enriched or MCP-depleted CMs were obtained according to the same procedure, but 10 mM CaCl₂ or 150 mg glucono-δ-lactone (GDL) were added to the milk after the chips have been immersed. One hour after addition of GDL or CaCl₂, the milk pH was 6.0 or 6.4, respectively. The control, MCP-enriched or MCP-depleted CMs were then gently rinsed with their corresponding MUF and kept in this solvent until analysis, to maintain mineral equilibria. For reaction with TG, 30 mL of a 60 g kg⁻¹ CM suspension was used to immerse the chips instead of skim milk. TG catalyzes isopeptidic cross-linking between polypeptide chains and these conditions are the result of a compromise between maximizing the internal cross-linking of the CMs and avoiding external cross-linking, especially with the whey proteins. An amount of 1 mg TG (100U/g, Ajinomoto Foods Europe, Paris, France) per 0.1 g of CMs was added to the pre-heated sample at 43 °C (Bahri et al., 2018) in which the chip was immersed. Cross-linking was performed at this temperature to optimize the enzymatic reaction. A control untreated sample received a volume of water equivalent to the volume of TG solution (100 μL) and both samples were stirred overnight at 43 °C. After cooling to room temperature, the chips were gently rinsed with control MUF and immediately analyzed with AFM in this medium. Successful cross-linking was evident as samples gelled if not stirred. Furthermore, the average hydrodynamic diameter of the TG-treated CMs increased from ~180 to ~250 nm (not shown; Bahri et al., 2018).

2.5. Size and mineral content of casein micelles in suspension

The mineral partition of the control, acidified and CaCl₂-supplemented skim milk was determined using a software for modelling mineral equilibria in milk, using the total ions concentration determined experimentally. The total ions concentration was taken from Bauland et al. (2020) as the same skim milk powder was used. Details about the software (Milk Salt GLM) and its validation can be found elsewhere (Bauland et al., 2020; Mekmene et al., 2009).

The hydrodynamic radius of CMs was measured by dynamic light scattering (DLS) using a Zetasizer Nano-ZS (Malvern Instruments, Malvern, UK). Milk samples were diluted (1:1000) in their respective MUF and measurements were carried out at 20 °C. The MUF viscosity was 1.187 mPa s at 20 °C.

2.6. Determination of the Young modulus of casein micelles using atomic force microscopy indentation

Indentation of the immobilized CMs was performed using a MLCT-D silicon nitride probe (Bruker Nano Surfaces, Santa Barbara, CA, USA) with a nominal spring constant $k = 0.03$ N m⁻¹ and a nominal tip radius $R = 20$ nm at the blunted apex, mounted onto an MFP3D-Bio Asylum Research atomic force microscope (Oxford Instruments, Santa Barbara, CA, USA). The exact spring constant of each cantilever was determined extemporaneously in control MUF at 20 °C, using the thermal method. The CM samples were then sequentially assessed in their corresponding MUF at 20 °C. The TG-treated sample was compared to the untreated control also incubated at 43 °C. Both were assessed in control MUF at 20 °C. A minimum of 3 repetitions was performed for each set (new milk
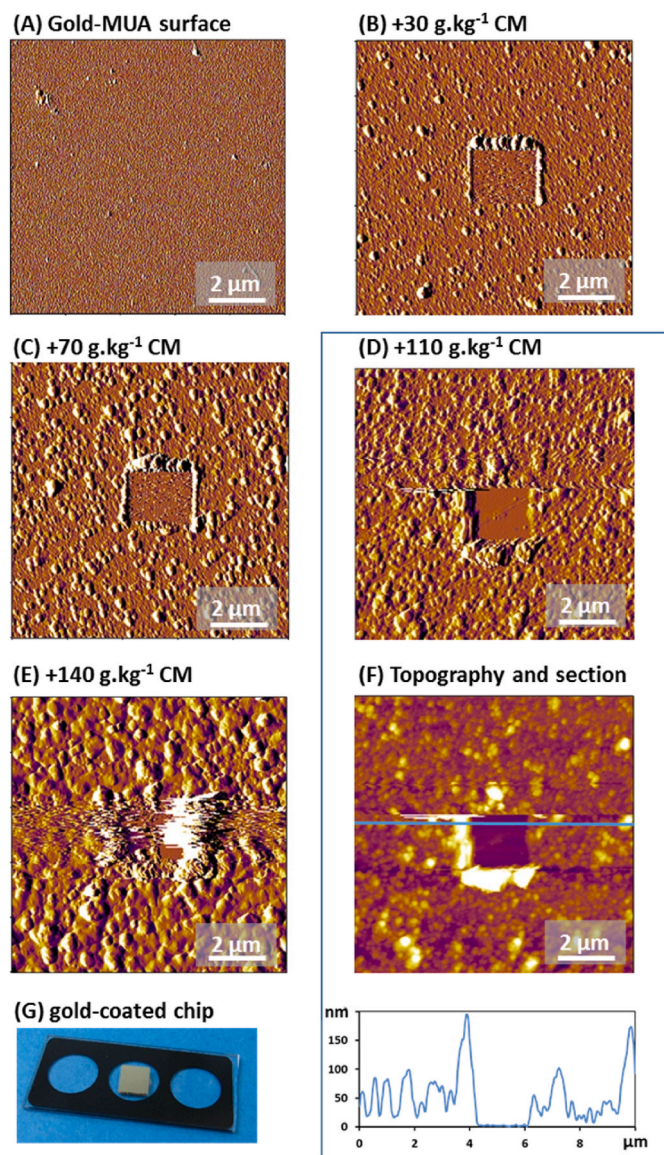
and MUF preparations, new chips, new probe). Force maps of 50×50 pixels were taken in $10 \times 10 \ \mu m^2$ sample areas and for conditions where a monolayer of CMs was expected on the chip surface (see results). The force-distance curves were taken at $1 \ \mu m \ s^{-1}$ speed rate, 500 pN maximum loading force and 500 nm withdrawal distance. They were fitted in batch using the Asylum Research software (version 14.20.152) and applying the Hertz model for mechanical contact between a sphere (here the tip) of radius R (m) and elastic surface:

$$F = kd = \frac{4E^*}{3}\sqrt{(R\delta^3)} \qquad (3)$$

where F is the loading force (N), d the cantilever deflection (m), k the spring constant of the cantilever (N.m^{-1}), δ the indentation (m) and E^* the complex Young modulus (Pa) with:

$$\frac{1}{E^*} = \frac{1 - \mu_{tip}^2}{E_{tip}} + \frac{1 - \mu_{sample}^2}{E_{sample}} \qquad (4)$$

where E_{tip} and E_{sample} are the moduli of the tip and of the sample, respectively, with Poisson's ratios associated with each object $\mu_{tip} = 0.25$ and $\mu_{sample} = 0.5$ (Uricanu et al., 2004). The curves were fitted over 85% of the total indentation, corresponding to $\delta < 25$–30 nm (Picas et al., 2012; Uricanu et al., 2004). Examples of fits can be found in supplementary data (Figure SI-2). After indentation measurements, the samples were rinsed, desiccated and imaged as in section 2.7 in order to check for the presence of the CM monolayer *a posteriori*.

2.7. Determination of an apparent contact angle using atomic force microscopy imaging

For the assessment of the apparent contact angle of individual CMs, the immobilized CMs were further gently rinsed with simulated milk ultrafiltrate (SMUF) to avoid the presence of lactose that crystallizes during drying. SMUF was obtained by adding, in this order, 1.58 g.L^{-1} KH$_2$PO$_4$, 1.20 g.L^{-1} K$_3$citrate·H2O, 1.79 g.L^{-1} Na$_3$citrate·2H$_2$O, 0.18 g.L^{-1} K$_2$SO$_4$, 1.00 g.L^{-1} CaCl$_2$, 0.65 g.L^{-1} MgCl$_2$·6H$_2$O, 0.30 g.L^{-1} K$_2$CO$_3$ and 0.60 g.L^{-1} KCl (Jenness & Koops, 1962). It was then adjusted to pH 6.7 or 6.0 with HCl or supplemented with 10 mM CaCl$_2$. In the latter case, the SMUF whitened due to calcium excess but it was used as such.

Slides were then left to dry in a desiccator for at least 6h. The remaining salt crystals were removed by depositing 1 drop of ultrapure water onto the slides for a few seconds, then re-drying the chips overnight. AFM imaging was performed in intermittent contact mode or "AC mode" using AC-240-TS silicon probe (Olympus Micro Cantilevers, Tokyo, Japan) with a nominal spring constant $k = 2 \ N \ m^{-1}$ and a nominal tip radius $R = 7$ nm. In $2 \times 2 \ \mu m^2$ images of the chip surface, sections were drawn across objects to measure their width w and height h, from which the apparent contact angle θ can be calculated as (Helstad et al., 2007; Silva et al., 2014):

$$\theta = \arccos\left(1 - \frac{h}{w}\right) \qquad (1)$$

The volume V of the spherical cap of width w and height h, calculated as:

$$V = \left(\frac{\pi h}{2}\right) \cdot \left(\frac{h^2}{3} + \left(\frac{w}{2}\right)^2\right) \qquad (2)$$

allowed the calculation of the radius of the equivalent sphere, i.e., of the equivalent volume taken by the CM in suspension (Gan et al., 2018; Ouanezar et al., 2012).

2.8. Statistics

A Student t-test was used to compare the apparent contact angle of the TG-treated versus untreated CMs. A one-factor analysis of variance or a Kruskal-Wallis non-parametric test were used for the Young modulus, the CMs radius and the apparent contact angle θ in order to evaluate the effect of the amount in MCP across the 3 samples investigated. Calculations were done using R (R Development Core Team (2010). R: A language and environment for statistical computing. R Foundation for Statistical Computing, Vienna, Austria. ISBN 3-900051-07-0, URL http://www.R-project.org).

3. Results and discussion

3.1. Surface coverage by casein micelles

Fig. 1A–E shows AFM amplitude images of the functionalized gold surface exposed or not to CM suspensions ranging from 30 to 140 g kg^{-1} and prepared for imaging in air as described above. Amplitude images result from recording of the AFM online corrections to set point and best render slopes and contours of the objects. As expected, increasing the CM concentration during exposure increases the density coverage of the chip. By scratching the sample over a $2 \times 2 \ \mu m^2$ area with the AFM tip at high loading force and then imaging a larger field, it is possible to use the height output of the AFM image to measure the thickness of the CM layer.

For the 110 g kg^{-1} CM concentration, the scratching reveals that the thickness is ~100 nm from the CMs apex and that the tip does not return to the substrate level between adjacent CMs (Fig. 1F, insight section). By comparison, the height of individual CMs deposited at 30 g kg^{-1} is $h = 46 \pm 18$ nm (N = 93; from data presented in Fig. 3). Performing a blind force map of a sample in order to get a significant number of indentation force curves on CMs – and as little as possible on the surrounding substrate – requires that CMs are immobilized as a uniform single layer. Immobilization of CMs at 110 g kg^{-1} appears to fulfill these conditions. This CM concentration probably prevents their spreading on the flat substrate, explaining that a lower height is found at 30 g kg^{-1} where CMs are individually resolved. At the greater concentration of 140 g kg^{-1}, the thickness of the CM layer is 150–200 nm (not shown), indicating piling of CMs, a situation that does not warrant the mechanical evaluation of CMs internal assembly.

Previous reports have shown that imaging CMs in liquid is a tedious task (Bahri et al., 2017; Ouanezar et al., 2012; Uricanu et al., 2004). AFM probes used for indentation typically have broad tips and soft cantilevers, making imaging difficult, and manual indentation reaches a limited numbers of force-curves, let's say a hundred over a reasonable amount of time. On the other hand, thousands of measurements are easily accessible through the proposed approach, to the expense of precise indentation at the apex of micelles. Close-packing of the CMs is also expected to prevent slippage of the AFM tip when pointing too close to the CM's side (Uricanu et al., 2004). As a result, it seems both reasonable and relevant to perform blind force maps using 110 g kg^{-1} CMs as an effective deposition concentration.
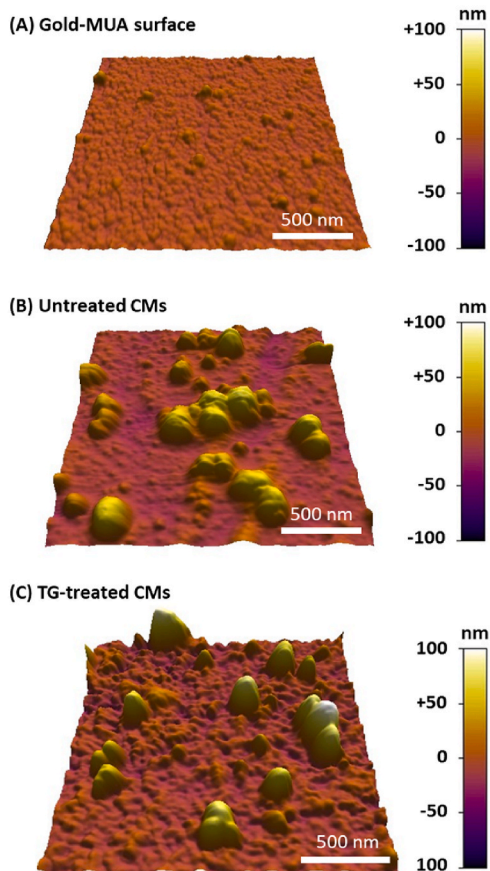
Note that for the second approach that consists in measuring contact angles of individual CMs, it is required that the CMs are sufficiently distant from one another to be able to measure h and w correctly. Therefore, in that case, a deposition concentration of 30 g kg^{-1} CMs was chosen, according to Fig. 1B.

3.2. Cross-linking with transglutaminase as a positive control for increased intra-micellar interactions

TG catalyzes the formation of covalent bounds between primary amines and γ-carboxamide groups of lysine and glutamine residues, respectively. The enzyme has been used in various food products including dairies, in order to control allergenicity, texture and water holding capacity of milk gels (Li & Zhao, 2019; Romeih & Walker, 2017). In the present study, TG treatment was used to cross-link caseins within CMs while limiting cross-links between CMs.

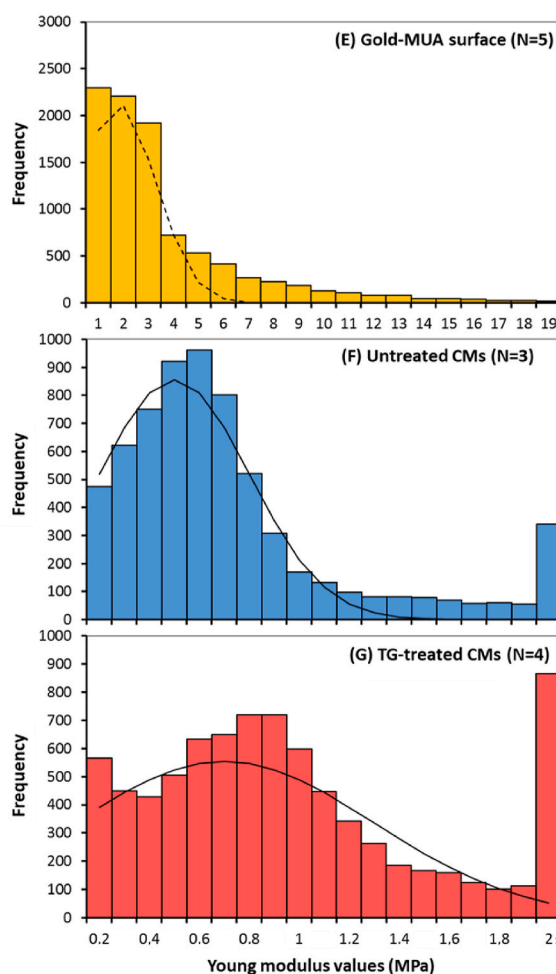Fig. 2 gives a comparison of AFM height images of a naked

Fig. 2. Mechanical properties of individual casein micelles (CMs) treated or not with transglutaminase (TG). Left panel: 2 × 2 μm² AFM height images of (A) the functionalized gold surface, (B) the same surface with immobilized untreated CMs at 30 g kg⁻¹ and (C) the same surface with immobilized CMs at 30 g kg⁻¹, further treated with TG. Left table (D) shows the average radius of equivalent sphere and the apparent contact angle θ for the untreated and TG-treated CMs. The images are recorded in air. Right panel: frequency histograms of the Young modulus values calculated over the force maps recorded onto (E) the functionalized gold surface, (F) the same surface with immobilized untreated CMs at 110 g kg⁻¹ and (G) the same surface with immobilized CMs at 110 g kg⁻¹, further treated with TG. Average values of Young moduli are displayed on the right table (D). The force maps are recorded in control milk ultrafiltration permeate (MUF) at 20 °C. Each histogram is the result of 3–5 repetitions (new sample, new chip, new probe, one force map). Black lines are the Gauss distributions that best fitted the data. Beware the change in x-scale between (E) and (F)/(G). (For interpretation of the references to colour in this figure legend, the reader is referred to the Web version of this article.)

functionalized gold surface (Fig. 2A) and gold surfaces exposed with 30 g kg⁻¹ untreated CMs (Fig. 2B) and TG-treated CMs (Fig. 2C), in air, and at the same XYZ scales. The average radius of the particles, calculated as that of the sphere of equivalent volume, is 57 ± 13 nm for untreated and 69 ± 15 nm for TG-treated CMs (Fig. 2D, ~93 particles imaged per condition), which is consistent with reported sizes of individual CMs (Bahri et al., 2018; Ouanezar et al., 2012; Silva et al., 2015). Meanwhile, hydrodynamic radii of 94 ± 3 nm were measured using DLS for untreated and 125 ± 10 nm for TG-treated CMs (not shown; N = 3 different suspensions × 3 dilutions × 10 measurements). It is expected that DLS intensity-average measurements yield larger radii than AFM measurements that are number-averaged. However, in both approaches, the TG-treated particles are larger than the untreated particles, which has already been observed and is probably the result of some limited protein

aggregation phenomena (Bahri et al., 2018).

The apparent contact angle of the individual CMs is $\theta = 39 \pm 7°$ for untreated and $\theta = 46 \pm 6°$ for TG-treated CMs (Fig. 2D), which goes along with the prominent aspect of TG-treated compared to untreated CMs, respectively (Fig. 2A and B). These values are lower than those previously found for cross-linked CMs ($\theta \sim 60°$) (Bahri et al., 2018), while those for untreated CMs agree with the 33–44° range of previous reports (Bahri et al., 2017; Silva et al., 2015). Yet, TG-treated CMs spread significantly less onto the gold substrate than do the untreated CMs (p≪0.001). Therefore, these results suggest that the cross-linked CMs have a greater rigidity than untreated ones, assuming that surface forces during adsorption are not influenced by the TG treatment (Evangelopoulos et al., 2012).

In an attempt to characterize the effect of TG on CMs in a more

Images of casein micelles in air (30 g.kg⁻¹)

(A) MCP-depleted CMs

(B) Control CMs
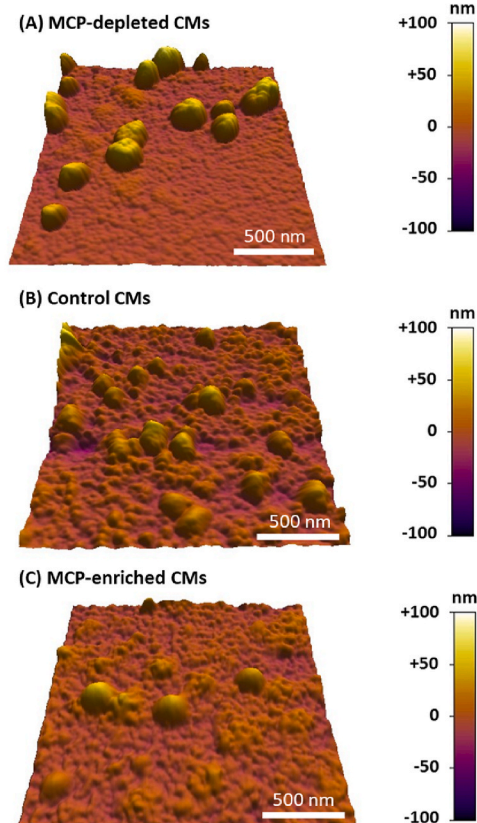
(C) MCP-enriched CMs

(D) Summary tables

N=93-125 micelles over 3-6 chips	MCP-depleted	Control	MCP-enriched	p-value
radius of equivalent sphere (nm)	51 ± 14[a]	57 ± 13[b]	65 ± 14[c]	8.2×10⁻¹¹
apparent contact angle (°)	38 ± 9[a]	39 ± 7[a]	35 ± 6[b]	2.6×10⁻³

Indentation of casein micelles in liquid (110 g.kg⁻¹)
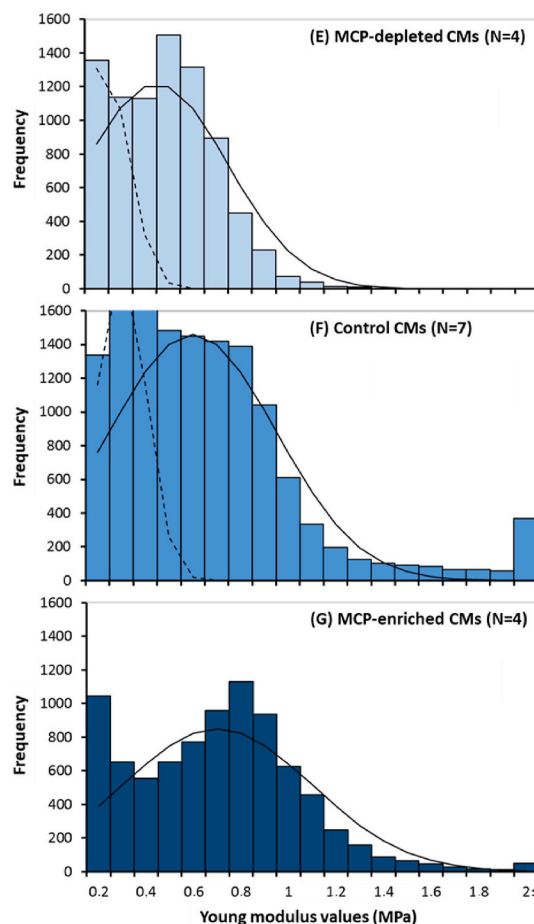
N=10,000 force curves over 4-7 chips	MCP-depleted	Control	MCP-enriched	p-value
Young modulus (MPa)	0.36 ± 0.24[a]	0.44 ± 0.35[b]	0.56 ± 0.40[c]	2.2×10⁻¹⁶

Fig. 3. Mechanical properties of individual casein micelles (CMs) with varying amount of micellar calcium phosphate (MCP). Left panel: 2×2 μm² images of (A) CMs at 30 g kg⁻¹, immobilized then depleted in MCP by acidification to pH 6.0 in skim milk environment, (B) immobilized control CMs at 30 g kg⁻¹ (pH 6.6) and (C) CMs at 30 g kg⁻¹, immobilized then enriched in MCP by addition of 10 mM CaCl₂ (pH 6.3) in skim milk environment. Additional images are displayed in Figure SI-1 in the supplementary data. Left table (D) shows the average radius of equivalent sphere and the apparent contact angle θ for the depleted, control and enriched CMs. The images are recorded in air. Right panel: frequency histograms of the Young modulus values calculated over the force maps recorded onto (E) CMs at 110 g kg⁻¹, immobilized then depleted in MCP by acidification to pH 6.0 in skim milk environment, (F) control immobilized CMs at 110 g kg⁻¹ (pH 6.6) and (G) CMs at 110 g kg⁻¹, immobilized then enriched in MCP by addition of 10 mM CaCl₂ (pH 6.3) in skim milk environment. Average values of Young moduli are displayed on the right table (D). The force maps are recorded in the corresponding milk ultrafiltration permeates (MUF) at 20 °C. Each histogram is the result of 4–7 repetitions (new sample, new chip, new probe, one force map). Black lines are the Gauss distributions that best fitted the data.

quantitative way, direct indentation measurements were performed by AFM force mapping onto CMs immobilized at 110 g kg⁻¹, in their natural MUF environment and at 20 °C (right panel of Fig. 2). For each sample, between 7,000 and 10,000 force curves were obtained over 3 to 5 chips. From the fitting of the force-distance curves, the Young moduli of untreated and TG-treated CM single layer were obtained. In the absence of CMs, the functionalized gold substrate exhibits Young modulus of up to 10 MPa (Fig. 2E) while thin gold film exhibits Young modulus in the order of GPa (Salvadori et al., 2003). The lower values observed here probably result from the presence of the self-assembled monolayer after reaction with mercaptoundecanoic acid and the immobilization of residual peptides contained in the MUF. Single layers of untreated CMs mostly exhibit Young modulus smaller than 1.2 MPa, except for one repetition in which some larger values are found. The average value is 0.65 ± 0.82 MPa (Fig. 2F), in agreement with

previously reported order of magnitude (Uricanu et al., 2004). Meanwhile, single layers of TG-treated CMs show a wider Young modulus distribution, with an average value of 0.80 ± 0.95 MPa and more frequent values larger than 1.2 MPa (Fig. 2G; p $= 2 \times 10^{-16}$). In Bahri's work, the Young modulus of untreated CMs was 0.27 ± 0.01 MPa (Bahri et al., 2017) while those of TG-treated CMs were unevenly distributed, with values of 0.22 ± 0.01, 0.54 ± 0.01 and 0.71 ± 0.01 MPa (Bahri et al., 2018). Nieuwland et al. (2015) also found an increase of the Young modulus of CMs with the degree of cross-linking by TG.

The present results confirm that indentation measurements by AFM are capable of quantifying mechanical differences between untreated and covalently cross-linked CMs by TG. The obtained distributions for the Young modulus are wide (Fig. 2) but this is not unexpected. It was shown that the Young modulus value is proportional to the CM size with a factor of ~2 (Uricanu et al., 2004). The variability of the

measurements is thus intrinsically large on a system that displays a wide size distribution. However, the force mapping approach over CM single layers allows the batch acquisition and treatment of thousands of force curves (N≃10,000). Such large number of repetitions makes the statistical tests very powerful and thus the characterization of fine variations between samples.

3.3. Effect of micellar calcium phosphate content on the properties of casein micelles

3.3.1. Size and mineral content of casein micelles in suspension

Besides covalent cross-linking of the CMs' internal structure, it is possible to tune the non-covalent interactions by modifying the amount of MCP within the CMs. MCP-depleted and MCP-enriched CMs were obtained by decreasing the pH of the milk used for equilibration from 6.6 to 6.0 or by adding 10 mM CaCl₂, respectively. Compare to the control CMs, MCP-depleted and MCP-enriched samples result in −18 and + 24% variations in MCP content, respectively, while both conditions increase the Ca-bound content (Table 1). After the immobilized CMs are equilibrated 1h with the control or modified skim milk (see section 2.4), it is assumed that their mineral content is identical to the CMs of the surrounding milk. DLS measurements performed on the control and modified skim milk show that the hydrodynamic radius of the CMs is not modified when the mineral content is varied within the range investigated (Table 1; p = 0.48). This is in accordance with the results of former studies (Philippe et al., 2005; Silva et al., 2013).

3.3.2. Mechanical properties

Fig. 3 shows the results of AFM imaging in air and of AFM indentation in MUF, when CMs are enriched or depleted in MCP after immobilization. Fig. 3A and C shows examples of 2 × 2 μm² AFM height images of CMs depleted or enriched in MCP, respectively, while the control is shown in Fig. 3B. The average radius of the individual CMs, calculated as that of the sphere of equivalent volume from the height images, was 57 ± 13 nm for control, against 51 ± 14 nm for MCP-depleted and 65 ± 14 nm for MCP-enriched CMs (Fig. 3D, between 93 and 125 particles imaged per condition). Therefore, using AFM imaging in air, the CMs exhibit a significantly larger radius as they contain more MCP (p = 8.2 × 10⁻¹¹) while no difference is found using DLS intensity measurements (Table 1). A possible explanation could be that the CMs containing more MCP are more resistant to abrasion during rinsing with MUF and SMUF. Thus, the drying step required for imaging in air may induce bias on the measure of the contact angle of CMs.

The apparent contact angle of the individual CMs is $\theta = 39 \pm 7°$ for control CMs, against $\theta = 38 \pm 9°$ for MCP-depleted CMs at pH 6.0 and $\theta = 35 \pm 6°$ for MCP-enriched CMs with 10 mM CaCl₂ (Fig. 3D). Counterintuitively, it therefore seemed that the MCP-enriched CMs spread slightly more on the functionalized surface than the control or MCP-depleted ones. It may indicate that the Young modulus of the MCP-enriched particles is lower if the surface forces are identical. In conditions where the release of MCP is extensive, such as after acidification to pH 5.2 or demineralization using 0.1 M citrate, single CMs exhibit lower θ values than control ones, which is interpreted as a decrease of rigidity (Silva et al., 2015).

Direct indentation measurements of CMs immobilized at 110 g kg⁻¹, performed at 20 °C and in the MUF corresponding to each MCP level, give Young moduli of 0.36 ± 0.24, 0.44 ± 0.35 and 0.56 ± 0.40 MPa for MCP-depleted, control and MCP-enriched CMs (Fig. 3E, F, 3G and 3D). Two repetitions of force maps over the control CMs and one over the MCP-depleted CMs resulted in unexpectedly low Young modulus values, thus accounting for the lower distributions centered on 0.3 MPa (dashed line in Figs. 3F) and 0.23 MPa (dashed line in Fig. 3E), respectively. However, all the data set was included for the calculation of the average moduli and the statistical tests. Overall, the results show that the Young moduli of the CMs significantly increases as their MCP content increases (p = 2.2 × 10⁻¹⁶).

Unlike the results of section 3.2, the contact angle and the indentation give contradictory results on the variation of the elasticity of CMs with the MCP content. However, as suggested from the discrepancies between the size obtained from DLS and AFM, the drying step applied before imaging in air might have induced some bias. Compared to TG treatment that forms covalent bonds, which are likely to be maintained during the drying step, dried CMs with modified MCP content might not be representative of their state in MUF. Therefore, the results obtained directly in MUF (i.e., the indentation results) appear to the author to be more reliable and indicate, for the tested conditions, that the Young modulus of CMs is positively correlated with their MCP content.

Away from the CM assembly, it has been shown that the addition of calcium and phosphate ions also increase the Young modulus of a layer of αₛ-casein deposited onto a polyelectrolyte film (Nagy et al., 2010). On the opposite, no difference in elasticity is reported when indenting CMs immobilized from skim milk acidified in the pH range 5.0–5.6 (Uricanu et al., 2004). In this pH range, the CMs contain about 0–50% of their total MCP compared to the physiological conditions (calculated with Milk Salt GLM). On the other hand, the same study reports larger Young moduli for control CMs at 20 °C, compared to those of CMs at 4 °C, which are expected to be about 15% depleted in calcium but also depleted in β-casein (calcium partition estimated from the data of Zulewska et al., 2018). Bahri et al. (2017) find an average modulus of 0.27 MPa for native CM (pH 6.6) which is comprised in the range [0.05–0.5] MPa measured by Uricanu et al. (2004) for acidified CMs (pH 5.2). Thus, the Young modulus of CMs change by less than one order of magnitude when they are fully depleted of MCP. However, considering the high number of CMs building the milk gel (~10¹⁷-10¹⁹ CMs per liter of milk), small but significant differences as the ones found in this study may have some relevance to explain the macroscopic properties of the gel.

MCP constitutes anchor points for phosphoserine residues of several casein polypeptide chains, strengthening bonds between casein monomers within the CMs. It has been reported that CMs under osmotic stress show soft compressible regions while harder ones resist to compression (Bouchoux et al., 2010). As the MCP exists as several hundreds of nanoclusters distributed within the hard regions, this suggests that MCP contribute, at least locally, to the rigidity of the CMs, which is consistent with the present results. The decrease in CM elasticity associated with a decrease of its MCP content is probably the consequence of a weakening of the nanocluster links between casein monomers. The increase of the Young modulus of CMs with the increase of their MCP content is more puzzling, as little is known about the newly formed MCP. To increase the elasticity and the number of bonds inside the CM, we assume that either an existing nanocluster grows in size and involves additional casein residues for its stabilization, or new nanoclusters are formed, which in turn involves the formation of new connections with casein residues. Recently, it was suggested that the existing nanoclusters would grow in size to accommodate the newly formed MCP (Wang et al., 2020).

From a methodological point of view, this extensive investigation of the use of AFM to assess the Young modulus of CMs reaches several points of conclusion. First, environmental or chemical modifications of already immobilized CMs is a convenient way to control surface coverage and prevent aggregation of the CMs, e.g. at pH 5.0 (Ouanezar et al., 2012) or after renneting (unpublished results). Second, a force-mapping of CMs immobilized as single layers is an efficient way to collect thousands of indentation curves over a short period of time for a given experimental set, and to probe small but significant differences of elasticity between control and modified CMs. Indeed, enough data have to be collected to compensate variabilities in CM size and in the position of the tip relative to the CM's apex, parameters that are known to affect the Young modulus values (Bahri et al., 2017; Uricanu et al., 2004). The approach based on the measurement of the contact angle of CMs was comparatively not as successful. It is possible to perform such measurements in liquid (Bahri et al., 2017, 2018; Ouanezar et al., 2012) but this is more challenging and extremely time-consuming with the AFM

type that we used.

Recent AFM developments such as peak-force tapping and other dynamic approaches open perspectives for combined high-speed imaging and viscoelasticity measurements based on the phase difference between the approach and retraction steps (Jones, 2016). Like in the present study, immobilization of a single layer of CMs would probably be adequate to perform such measurements. Many biological systems display both elastic and viscous behaviors where Hertzian contact theory only deals with elastic objects. One element suggesting that CM behaves as a viscoelastic material is the hysteresis between the approach and retraction curves during indentation, indicating that the object may have flowed during the test (Figure SI-3 in supplementary data). A precise characterization of the viscoelastic properties of CM and of its relaxation behavior is a nice perspective that could give more information about the relationships between milk gel properties and the elementary bricks.

4. Conclusions

Blind force mapping of CMs immobilized as a single layer and modified after immobilization offers several advantages over indentation of individual CMs to measure their mechanical properties. The coverage density is standardized and a large number of data can be collected within a shorter period of time than in situations where single objects must be targeted, which promotes statistical robustness. This approach is successful in discriminating the Young modulus of CMs reticulated by TG or with modified MCP content (in the range - 18% to + 24% compared to the control). For the tested conditions (pH 6.6, pH 6.0 and + 10 mM $CaCl_2$), the Young modulus of CMs was anti-correlated to their MCP content. Thus, the variations in milk mineral equilibria encountered in cheese manufacture affect the mechanical properties of CMs. This result could help understanding the rheology of the enzymatic milk gel and its behavior during aging.

Sample credit author statement

Julien Bauland: Conceptualization, Writing - Original Draft, Data curation, Formal analysis, Investigation **Antoine Bouchoux**: Methodology, Validation, Writing - Review & Editing **Thomas Croguennec**: Conceptualization, Writing - Review & Editing, Supervision **Marie-Hélène Famelart**: Conceptualization, Writing - Review & Editing, Supervision **Fanny Guyomarc'h**: Conceptualization, Methodology, Writing - Original Draft, Data curation, Formal analysis, Investigation, Supervision.

Declaration of competing interest

None.

Acknowledgments

Appendix A. Supplementary data

Supplementary data to this article can be found online at https://doi.org/10.1016/j.foodhyd.2022.107577.

References

Bahri, A., Martin, M., Gergely, C., Marchesseau, S., & Chevalier-Lucia, D. (2018). Topographical and nanomechanical characterization of casein nanogel particles using atomic force microscopy. *Food Hydrocolloids, 83*, 53–60. https://doi.org/10.1016/j.foodhyd.2018.03.029

Bahri, A., Martin, M., Gergely, C., Pugnière, M., Chevalier-Lucia, D., & Marchesseau, S. (2017). Atomic force microscopy study of the topography and nanomechanics of casein micelles captured by an antibody. *Langmuir, 33*(19), 4720–4728. https://doi.org/10.1021/acs.langmuir.7b00311

Bauland, J., Famelart, M. H., Bouhallab, S., Jeantet, R., Roustel, S., Faiveley, M., & Croguennec, T. (2020). Addition of calcium and magnesium chlorides as simple means of varying bound and precipitated minerals in casein micelle: Effect on enzymatic coagulation. *Journal of Dairy Science, 103*(11), 9923–9935. https://doi.org/10.3168/jds.2020-18749

Bauland, J., Gaucheron, F., & Croguennec, T. (2022). Milk salt composition, distribution and analysis. In *Encyclopedia of dairy sciences* (pp. 941–953). Academic Press. https://doi.org/10.1016/b978-0-12-818766-1.00262-2.

Benitez, R., & Toca-herrera, J. L. (2014). Looking at cell mechanics with atomic force microscopy: Experiment and theory. *Microscopy Research and Technique, 77*(11), 947–958. https://doi.org/10.1002/JEMT.22419

Bouchoux, A., Gésan-Guiziou, G., Pérez, J., & Cabane, B. (2010). How to squeeze a sponge: Casein micelles under osmotic stress, a SAXS study. *Biophysical Journal, 99* (11), 3754–3762. https://doi.org/10.1016/J.BPJ.2010.10.019

Cipelletti, L., Manley, S., Ball, R. C., & Weitz, D. A. (2000). Universal aging features in the restructuring of fractal colloidal gels. *Physical Review Letters, 84*(10), 2275–2278. https://doi.org/10.1103/PhysRevLett.84.2275

Cooke, D. R., & McSweeney, P. L. H. (2014). The influence of alkaline earth metal equilibria on the rheological properties of rennet-induced skim milk gels. *Dairy Science & Technology, 94*(4), 341–357. https://doi.org/10.1007/s13594-014-0166-5

Dalgleish, D. G. (1983). Coagulation of renneted bovine casein micelles: Dependence on temperature, calcium ion concentration and ionic strength. *Journal of Dairy Research, 50*(3), 331–340. https://doi.org/10.1017/S0022029900023165

Evangelopoulos, A. E. A. S., Glynos, E., Madani-Grasset, F., & Koutsos, V. (2012). Elastic modulus of a polymer nanodroplet: Theory and experiment. *Langmuir, 28*(10), 4754–4767. https://doi.org/10.1021/LA2049037

Fagan, C. C., O'Callaghan, D. J., Mateo, M. J., & Dejmek, P. (2017). The syneresis of rennet-coagulated curd. In (4th ed.,, *Vol. 1. Cheese: Chemistry, physics and microbiology* (pp. 145–177). Elsevier Inc. https://doi.org/10.1016/B978-0-12-417012-4.00006-5.

Gan, C., Wang, K., Tang, Q., & Chen, Y. (2018). Comparative investigation on the sizes and scavenger receptor binding of human native and modified lipoprotein particles with atomic force microscopy. *Journal of Nanobiotechnology, 16*(1), 1–11. https://doi.org/10.1186/s12951-018-0352-3

Helstad, K., Rayner, M., van Vliet, T., Paulsson, M., & Dejmek, P. (2007). Liquid droplet-like behaviour of whole casein aggregates adsorbed on graphite studied by nanoindentation with AFM. *Food Hydrocolloids, 21*(5–6), 726–738. https://doi.org/10.1016/j.foodhyd.2006.10.006

Holt, C., Carver, J. A., Ecroyd, H., & Thorn, D. C. (2013). Invited review: Caseins and the casein micelle: Their biological functions, structures, and behavior in foods. *Journal of Dairy Science, 96*(10), 6127–6146. https://doi.org/10.3168/JDS.2013-6831

Holt, C., Davies, D. T., & Law, A. J. R. (1986). Effects of colloidal calcium phosphate content and free calcium ion concentration in the milk serum on the dissociation of bovine casein micelles. *Journal of Dairy Research, 53*(4), 557. https://doi.org/10.1017/S0022029900033082

Horne, D. S. (2020). Casein micelle structure and stability. In *Milk proteins* (pp. 213–250). Elsevier. https://doi.org/10.1016/b978-0-12-815251-5.00006-2.

Horne, D. S., & Lucey, J. A. (2014). Revisiting the temperature dependence of the coagulation of renneted bovine casein micelles. *Food Hydrocolloids, 42*, 75–80. https://doi.org/10.1016/j.foodhyd.2013.12.021

Jenness, R., & Koops, J. (1962). Preparation and properties of a salt solution which simulates milk ultrafiltrate. *Netherlands Milk and Dairy Journal, 16*, 153–164.

Jones, O. G. (2016). Developments in dynamic atomic force microscopy techniques to characterize viscoelastic behaviors of food materials at the nanometer-scale. *Current Opinion in Food Science, 9*, 77–83. https://doi.org/10.1016/j.cofs.2016.09.008

Kim, S., Lee, Y., Lee, M., An, S., & Cho, S. J. (2021). Quantitative visualization of the nanomechanical young's modulus of soft materials by atomic force microscopy. *Nanomaterials, 11*(6), 1593. https://doi.org/10.3390/nano11061593

de Kruif, C. (1999). Casein micelle interactions. *International Dairy Journal, 9*(3–6), 183–188. https://doi.org/10.1016/S0958-6946(99)00058-8

Li, Q., & Zhao, Z. (2019). Acid and rennet-induced coagulation behavior of casein micelles with modified structure. *Food Chemistry, 291*, 231–238. https://doi.org/10.1016/J.FOODCHEM.2019.04.028

Martin, A. H., Douglas Goff, H., Smith, A., & Dalgleish, D. G. (2006). Immobilization of casein micelles for probing their structure and interactions with polysaccharides using scanning electron microscopy (SEM). *Food Hydrocolloids, 20*(6), 817–824. https://doi.org/10.1016/J.FOODHYD.2005.08.004

Mekmene, O., Le Graët, Y., & Gaucheron, F. (2009). A model for predicting salt equilibria in milk and mineral-enriched milks. *Food Chemistry, 116*(1), 233–239. https://doi.org/10.1016/J.FOODCHEM.2009.02.039

Mellema, M., Walstra, P., van Opheusden, J. H., & van Vliet, T. (2002). Effects of structural rearrangements on the rheology of rennet-induced casein particle gels. *Advances in Colloid and Interface Science, 98*(1), 25–50. https://doi.org/10.1016/S0001-8686(01)00089-6

Nagy, K., Pilbat, A. M., Groma, G., Szalontai, B., & Cuisinier, F. J. G. (2010). Casein aggregates built step-by-step on charged polyelectrolyte film surfaces are calcium

phosphate-cemented. *Journal of Biological Chemistry, 285*(50), 38811–38817. https://doi.org/10.1074/jbc.M110.151167

Nieuwland, M., Bouwman, W. G., Bennink, M. L., Silletti, E., & Jongh, H. H. J. de (2015). Characterizing length scales that determine the mechanical behavior of gels from crosslinked casein micelles. *Food Biophysics, 10*(4), 416–427. https://doi.org/10.1007/S11483-015-9399-Y

Obeid, S., & Guyomarc'h, F. (2020). Atomic force microscopy of food assembly: Structural and mechanical insights at the nanoscale and potential opportunities from other fields. *Food Bioscience, 36*(May), 100654. https://doi.org/10.1016/j.fbio.2020.100654

Ouanezar, M., Guyomarc'h, F., & Bouchoux, A. (2012). AFM imaging of milk casein micelles: Evidence for structural rearrangement upon acidification. *Langmuir, 28*(11), 4915–4919. https://doi.org/10.1021/la3001448

Philippe, M., Gaucheron, F., Le Graet, Y., Michel, F., & Garem, A. (2003). Physicochemical characterization of calcium-supplemented skim milk. *Le Lait, 83*(1), 45–59. https://doi.org/10.1051/lait:2002049

Philippe, M., Le Graët, Y., & Gaucheron, F. (2005). The effects of different cations on the physicochemical characteristics of casein micelles. *Food Chemistry, 90*(4), 673–683. https://doi.org/10.1016/J.FOODCHEM.2004.06.001

Picas, L., Milhiet, P. E., & Hernández-Borrell, J. (2012). Atomic force microscopy: A versatile tool to probe the physical and chemical properties of supported membranes at the nanoscale. *Chemistry and Physics of Lipids, 165*(8), 845–860. https://doi.org/10.1016/J.CHEMPHYSLIP.2012.10.005

Romeih, E., & Walker, G. (2017). Recent advances on microbial transglutaminase and dairy application. *Trends in Food Science & Technology, 62*, 133–140. https://doi.org/10.1016/J.TIFS.2017.02.015

Salvadori, M. C., Brown, I. G., Vaz, A. R., Melo, L. L., & Cattani, M. (2003). Measurement of the elastic modulus of nanostructured gold and platinum thin films. *Physical Review B: Condensed Matter and Materials Physics, 67*(15). https://doi.org/10.1103/PhysRevB.67.153404

Silva, N. N., Bahri, A., Guyomarc'h, F., Beaucher, E., & Gaucheron, F. (2015). AFM study of casein micelles cross-linked by genipin: Effects of acid pH and citrate. *Dairy Science & Technology, 95*(1), 75–86. https://doi.org/10.1007/s13594-014-0199-9

Silva, N. N., Piot, M., de Carvalho, A. F., Violleau, F., Fameau, A.-L., & Gaucheron, F. (2013). pH-induced demineralization of casein micelles modifies their physicochemical and foaming properties. *Food Hydrocolloids, 32*(2), 322–330. https://doi.org/10.1016/J.FOODHYD.2013.01.004

Silva, N. N., Saint-Jalmes, A., de Carvalho, A. F., & Gaucheron, F. (2014). Development of casein microgels from cross-linking of casein micelles by genipin. *Langmuir, 30*(34), 10167–10175. https://doi.org/10.1021/la502274b

Uricanu, V. I., Duits, M. H. G., & Mellema, J. (2004). Hierarchical networks of casein proteins: An elasticity study based on atomic force microscopy. *Langmuir, 20*(12), 5079–5090. https://doi.org/10.1021/la0363736

van Vliet, T., van Dijk, H. J. M. M., Zoon, P., & Walstra, P. (1991). Relation between syneresis and rheological properties of particle gels. *Colloid & Polymer Science, 269*(6), 620–627. https://doi.org/10.1007/BF00659917

Walstra, P., van Dijk, H., & Geurts, T. (1985). The syneresis of curd. 1. General considerations and literature review. *Netherlands Milk and Dairy Journal, 39*(4), 209–246. https://agris.fao.org/agris-search/search.do?recordID=NL8600289.

Wang, Q., Holt, C., Nylander, T., & Ma, Y. (2020). Salt partition, ion equilibria, and the structure, composition, and solubility of micellar calcium phosphate in bovine milk with added calcium salts. *Journal of Dairy Science, 103*(11), 9893–9905. https://doi.org/10.3168/jds.2020-18829

Wu, Q., Van Der Gucht, J., & Kodger, T. E. (2020). Syneresis of colloidal gels: Endogenous stress and interfacial mobility drive compaction. *Physical Review Letters, 125*(20), 1–6. https://doi.org/10.1103/PhysRevLett.125.208004

Zulewska, J., Kowalik, J., Lobacz, A., & Dec, B. (2018). Short communication: Calcium partitioning during microfiltration of milk and its influence on rennet coagulation time. *Journal of Dairy Science, 101*(12), 10860–10865. https://doi.org/10.3168/jds.2018-14830